Exploring Phonon Interference: Insights From a Nano-Scale Silicon Double Slit Atomistic Simulation

Efstratios Nikidis, Paul Desmarchelier, Yoshiaki Nakamura, Anne Tanguy, Konstantinos Termentzidis, Joseph Kioseoglou

ADVANCED THEORY AND SIMULATIONS
www.advtheorysimul.com

Exploring Phonon Interference: Insights From a Nano-Scale Silicon Double Slit Atomistic Simulation

*Efstratios Nikidis, Paul Desmarchelier, Yoshiaki Nakamura, Anne Tanguy, Konstantinos Termentzidis, and Joseph Kioseoglou**

In this study, the classic double-slit experiment, originally developed for light waves is successfully adapted, to investigate the behavior of phonons in crystalline silicon. Through molecular dynamics (MD) simulations, how phonons can exhibit wave-like interference patterns when passing through two slits in a silicon block is explored. The results indicate that phonon waves behave similarly to photons, with slit distinct interference patterns. By manipulating geometric parameters such as slit width, distance, and length, in fringe distances that align with Young's double slit formula is observed to change. Key findings include the observation of phonon interference and the sensitivity of fringe distances to geometric configurations. Although some discrepancies with theory arose due to noise in the MD simulations, these results underscore the complexity of simulating phonon behavior in nanostructures. This study demonstrates that phonon behavior at the nanoscale can mirror classical wave interference phenomena, paving the way for future work that includes conducting physical experiments for validation and ultimately aiming to engineer devices that harness phononic interference for innovative applications in thermal management, microelectronics, and quantum computing.

1. Introduction

To exploit heat-transfer mechanisms and engineer efficient nanocomposites or other nanostructured materials, first there is a need to study, monitor, and understand their transport properties in depth. Direct or indirect control of energy flow has long been essential, even for what, by today's standards, are simple applications. Over the past century electron steering was discovered by manipulating their natural pathways,[1] laying the foundation for computer science[2] later that control was extended to light[3,4] and more recently to phonons[5–8] leading in an era of nano-engineered materials capable of controlling heat dissipation. In parallel, several intriguing heat-transport phenomena[9,10] which lie beyond the classical Fourier law[11,12] of conduction, have been observed or proposed, including thermal rectification[13–15] phonon filtering[16,17] and phonon diffraction.[18]

Innovative heat-transport phenomena therefore form the cutting-edge frontier of thermal management and energy-efficiency research. Wave-based phonon effects, in particular, stand out for their potential to revolutionize applications ranging from solid-state devices to high-temperature industrial processes. Among these effects, diffraction and rectification are fundamental to the transport of phonons, photons, and electrons. Diffraction arises when an energy carrier encounters an obstacle or aper-

E. Nikidis, J. Kioseoglou
Physics Department
Aristotle University of Thessaloniki
Thessaloniki GR-54124, Greece
E-mail: sifisl@auth.gr

E. Nikidis, J. Kioseoglou
Center for Interdisciplinary Research and Innovation
Aristotle University of Thessaloniki
Thessaloniki GR-57001, Greece

P. Desmarchelier, K. Termentzidis
University of Lyon
CNRS
INSA Lyon
CETHIL
UMR5008, Villeurbanne 69621, France

Y. Nakamura
Graduate School of Engineering Science
Osaka University 1–3 Machikaneyama-cho
Toyonaka, Osaka 560-8531, Japan

A. Tanguy
Université de Lyon
INSA Lyon
CNRS
LaMCoS
UMR5259, Villeurbanne 69621, France

The ORCID identification number(s) for the author(s) of this article can be found under https://doi.org/10.1002/adts.202500504

DOI: 10.1002/adts.202500504

Table 1. Phonon coherent and incoherent transport mechanisms.

Property	Coherent Phonon Trasport	Incoherent Phonon Transport
Phase Information	Preserved.	Lost due to scattering.
Transport Type	Ballistic, wave-like (non-diffusive)	Diffusive (random, governed by classical laws like Fourier's)
Scattering Events	Rare, and when they do occur, preserve phase information.	Frequent, random scattering events (impurities, boundaries, etc.).
Wave-like Phenomena	Diffraction, interference, tunnelling, thermal bandgaps.	No wave-like behaviors, phonons behave like particles.
Regimes	Occurs at small scales, low temperatures, or very clean materials.	Occurs at larger scales or higher temperatures.

ture, causing it to bend and interfere, thereby shaping its flow and effective transport properties. Rectification, by contrast, denotes an asymmetric energy flux – transport that is more efficient in one direction than the other. This behavior appears in thermal systems, where phonons can sustain directional heat flow, and in electronic circuits, where diodes enforce unidirectional current. Both phenomena leverage the wave-like nature of their carriers to control and manipulate transport in engineered materials.

In nanostructures, heat transport is commonly tuned through atomic-scale interfaces,[19] pores,[20,21] dopants,[22] and similar features. When the characteristic dimensions of these phonon-scattering centres are smaller than the phonon mean free path, transport falls into the classical diffusive regime: Fourier's law applies, and phase information is lost through diffuse boundary scattering and internal processes such as Umklapp phonon–phonon and phonon – impurity interactions.[23]

Although incoherent scattering dominates the diffusive regime, coherent effects re-emerge at the nanoscale and at low temperatures. The wave-like nature of phonons then gives rise to coherence, band-gap formation, diffraction, interference, and even a coherent thermal-hydrodynamic regime.[24] Unlike photons—whose coherence properties were established a century ago—and electrons, whose wave character has long been exploited, our understanding of phonon coherence remains incomplete. Yet phonons are equally fundamental carriers of energy and information, and uncovering how coherence shapes thermal conduction will be crucial for the next generation of heat-control and management technologies.[25]

Coherence effects (**Table 1**) concerning phonons were proved mostly either theoretically or numerically and less experimentally and they were oriented in meta structures like superlattices or periodic perforated or with pillars membranes and nanowires. The coherency is expressed by the energy gap opening, the modification of the phonon velocity, the suppression of the effective thermal conductivity, the appearance of non-diffusive transport regimes like ballistic and hydrodynamic, or the appearance of phonon tunnelling and phonon diffraction and interference.

Manipulating phonon paths can control heat transfer. For instance, Dai et al.[26] showed that applying external stress or strain tunes thermal conductivity by changing the density of twin boundaries, creating a mechanically controlled thermal switch with hysteresis. Maldovan[27] discusses creating forbidden energy bandgaps for thermal phonons through wave interference, thereby manipulating heat transport. Seif et al.[28] proposed an engineered nanostructure with tunable, non-reciprocal phonon transport achieved via optomechanical coupling, useful for an acoustic isolator or thermal diode. Molecular-dynamics (MD) simulations remain a powerful tool for studying phonon behavior. Although real systems include uncertainties such as temperature fluctuations, crystal disorder, and quantum effects, MD still provides a valuable window into the fundamental nature of phonons and their interactions in nanomaterials.

Thomas Young's double-slit experiment, conducted in the early 1800s, demonstrated the wave nature of light and laid the foundation for quantum mechanics.[29] By passing light through two closely spaced slits, Young observed an interference pattern, indicating that light behaves as a wave. This experiment challenged the prevailing particle view of light and contributed to the concept of wave-particle duality.[29] The notion of coherence originated with Young's work: interference fringes appear only when photons remain phase-correlated. Interferometers have since demonstrated coherence in wave fields ranging from light[30] to acoustics.[31] The first clear evidence of phonon interference, a high-frequency propagating-wave analogue, appeared much later; Anderson and Sabisky's study[32] is widely cited as one of the earliest accounts.

In our earlier research,[33] we demonstrated how voids and amorphous patches create diffraction and interference patterns consistent with the Fresnel–Kirchhoff equation, emphasizing the significance of these patterns for understanding phonon behavior in crystalline silicon (Si). In this context, the "double slit experiment"[29] pioneered by Tomas Young in the field of optics serves as an intriguing analogy for studying the behavior of phonons. We aim to transition from the general framework of the Fresnel-Kirchhoff diffraction theory to the more specific case of Young's double-slit experiment, focusing on the nuanced behavior of phonon. The double-slit experiment by Thomas Young demonstrated the wave nature of light. In the experiment, light passes through two closely spaced slits, creating an interference pattern of bright and dark fringes two slits overlap, producing constructive and destructive on a screen. This pattern occurs because light waves from the interference. The positions of bright fringes (constructive interference) are given by the equation:

$$d \sin(\theta) = m\lambda \tag{1}$$

where:

- d: Distance between the slits
- θ: Angle of the fringe from the central axis
- m: Fringe order (an integer, m = 0, ±1, ±2, ...)
- λ: Wavelength of the light

For dark fringes (destructive interference), the equation is:

$$d \sin(\theta) = (m + 1/2)\,\lambda \tag{2}$$

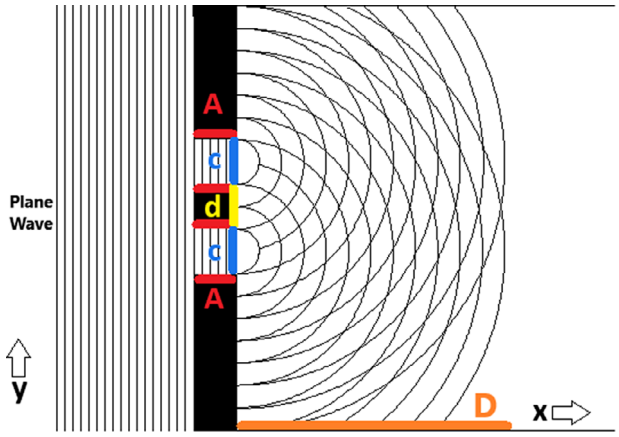

Figure 1. A simple schematic of the geometry that was used for the MD simulations. Slit length (A, red). Slit distance (d, yellow), Slit width (c, blue).

Building on this foundation, the present study adapts the classic double-slit experiment to investigate phononic wave interference directly, revealing that phonons can display interference patterns akin to light waves. This exploration not only reinforces the importance of geometric configuration in shaping phonon behavior but also pinpoints a specific propagation frequency that maximizes coherence and interference. Phonons can be conceptualized as waves travelling through the crystal lattice, carrying energy, momentum, and information. Their dispersion relations, group velocities, and wavelengths depend on the crystal structure and elastic properties of the host material. Taken together, these considerations underline the critical role of phonon-interference phenomena in advancing our understanding of thermal transport and in designing materials for phononic devices and thermal-management technologies.

Recent reviews underscore the importance of phonons' wave-like attributes[34] and when interference patterns are controlled, offer spatial control over energy transfer. Because terahertz excitations can be generated and propagated in crystalline or amorphous silicon[35] it is natural to recreate a double-slit experiment in molecular-dynamics (MD) form. Analogously to Young's optical setup, our nano-scale silicon sample with two slits (**Figure 1**) allows us to examine the interference fringes formed by diffracted phonons. The propagating lattice excitation is modelled as a Gaussian-ramped sinusoidal drive,[36] producing a deterministic evolution in the MD simulation. In the simulation box generated by LAMMPS, every atom's coordinates are predefined for each time-step after relaxation. The paper is organized as follows: first, we detail the quasi-monochromatic wave-packet methodology and the nanostructure models (a flow chart is provided in Figure S2, Supporting Information). We then present the frequency-dependent simulation results and compare them with Young's equation. Finally, the main findings are summarized in the conclusions.

2. Methodology

Various silicon crystal blocks with systematically varied geometries were generated. Each sample is based on diamond-cubic Si and replicates the key elements of Thomas Young's double-slit experiment: the silicon lattice provides the propagation medium, while two void regions act as slits. In blocks oriented with the (100) axis along z, a slice of thickness A is removed, leaving two open channels (Figure 1). To map the resulting interference, we vary three geometric parameters (Table 1):

W• Slit length, A
• Slit spacing, d
• Slit width, c

After construction, each configuration (**Table 2**) is annealed in an isothermal – isobaric (NPT) ensemble. The simulations are run in LAMMPS[37] at 100K and ambient pressure, with temperature and pressure controlled by the Nosé – Hoover thermostat – barostat pair. Interatomic forces are described by the modified Stillinger- Weber potential for crystalline Si.[38] For the faces perpendicular to the wave-propagation direction we tested both periodic and free (non-periodic) boundary conditions, while the remaining faces were kept periodic.

Once relaxation is complete, we identify the source frequency that yields the clearest interference. A sweep from 1 THz to 6 THz is performed on the reference geometry ($Geometry\ 1: A = 4\ nm, d = 8.6\ nm, c = 3\ nm$).

These preliminary tests (see **Figure 2**) allow us to observe how each frequency interacts with the material's structure and identify the frequency that leads to the most effective propagation. The geometry chosen for the frequency study is Geometry 1 and it was chosen due to the least extreme geometrical characteristics. Once the optimal frequency is established, the next step is to proceed and explore the influence of different geometric configurations on the propagation dynamics. In this case this optimal frequency is 6THz producing the clearer phonon interference pattern. This simulation was down at 0 K (initially) with no thermosetting, the only source of energy is the forced imposed to excite atom.

The molecular-dynamics simulations reported in this work all start from an equilibrated 0 K lattice. To monitor any subsequent heating, we record at every time step the instantaneous kinetic temperature:

$$T(t) = \frac{2}{3k_B} E_{kin}(t) \tag{3}$$

where E_{kin} is the total kinetic energy and k_B is Boltzmann's constant, for each atomistic configuration. The Gaussian-ramped sinusoidal drive has a peak force of $F_0 = 6.05 \times 10^{-13}\ N$, which, through Hooke's law with $k_2 = 60.9\ N\ m^{-1}$, produces a maxi-

Table 2. The different geometrical cases tested.

Case No	Purpose of the study	A [nm]	d [nm]	c [nm]
1	Study of the effect of thickness of barrier (A).	4 nm	8.6 nm	3 nm
2		8 nm	8.6 nm	3 nm
3		12 nm	8.6 nm	3 nm
4	Study of the effect of the two slits distance (d)	4 nm	4 nm	3 nm
5		4 nm	20 nm	3 nm
6	Study of the effect of the slits thickness (c).	4 nm	8.6 nm	1 nm
7		4 nm	8.6 nm	5 nm

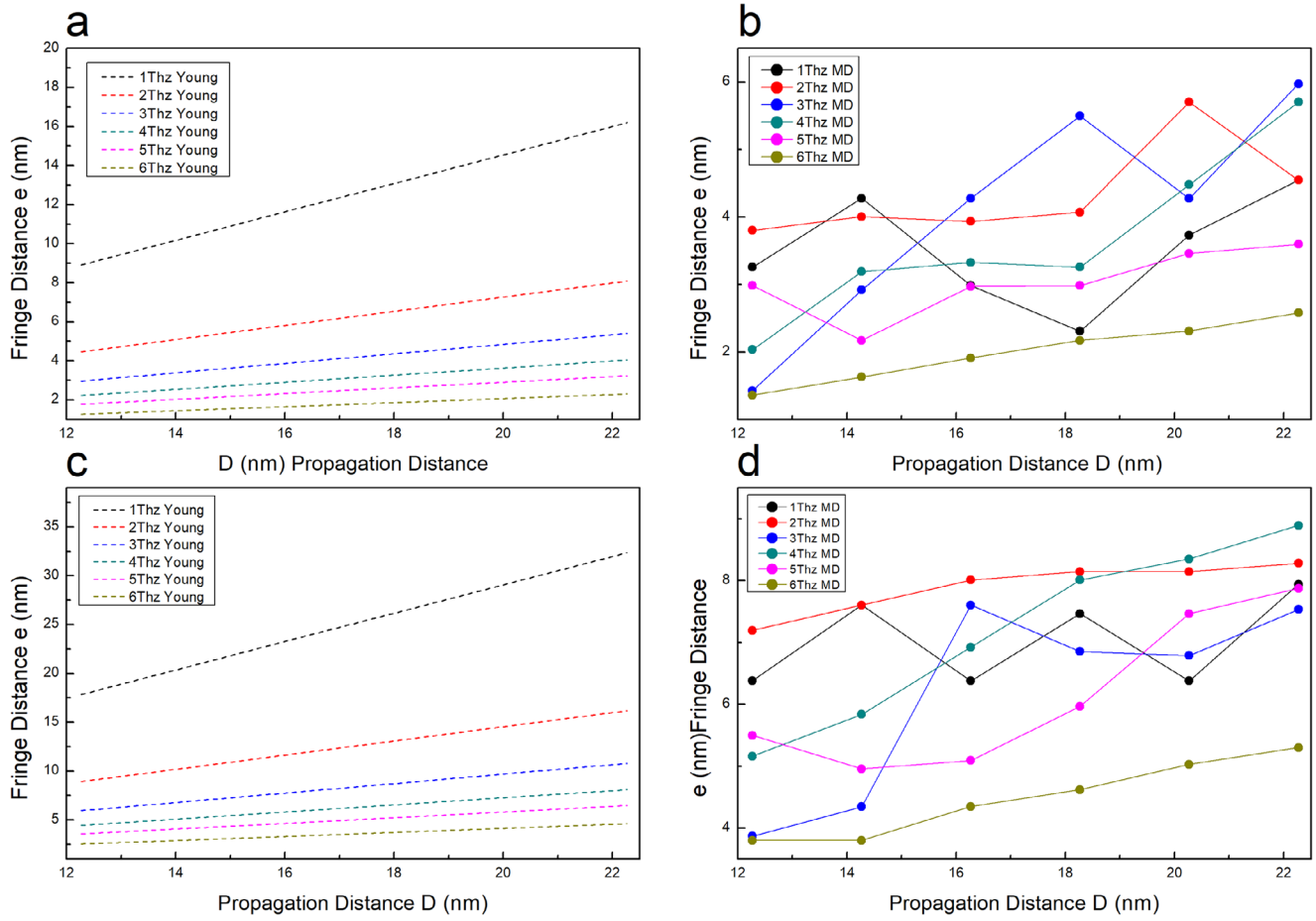

Figure 2. Frequency analysis scatter plots of fringe distance versus propagation distance. a): Analytical solution of Young's equation for $m = 1$. b): Molecular dynamics results for $m = 1$. c): Analytical solution of young equation for $m = 2$. d): Molecular dynamics results for $m = 2$.

mum displacement $x_{max} = 9.9 \times 10^{-5}$ ∀ ($strain$ 1.8×10^{-5}). This is ∼ 300× below the lowest reported anharmonic threshold for Si ($\varepsilon \simeq 0.5\%$),[39] ensuring purely harmonic response. The harmonic driving variable "amp" in our LAMMPS script is defined as:

$$amp\,(t) = A_0 \sin\left(\omega\left(t - t_0\right)\right) \times \left[\Theta\left(t_0 - t\right) \exp\left(-\frac{\left(t - t_0\right)^2}{2\tau^2}\right) + \Theta\left(t - t_0\right)\right] \quad (4)$$

where $A_0 = 3.773 \times 10^{-4}$ (amplitude coefficient), $\omega = \nu_w$ (pulse angular frequency), $t_0 = 3\nu_\tau$ (Gaussian center time), and $\tau = \nu_\tau$ (Gaussian width parameter).

with

$$\Theta\,(x) = \begin{cases} 1, & x > 0 \\ 0, & x \le 0 \end{cases} \quad (5)$$

For our 0 K, non-thermostatted runs at 6 THz over 100 ps (≈600 drive cycles), the instantaneous kinetic temperature, exhibits brief spikes no larger than 10^{-5}–10^{-4} K at the start of each half-cycle (see **Figure 3**). Consequently, the system remains effectively cryogenic, anharmonic scattering is suppressed, and the clear phonon double-slit fringes we observe must arise from purely coherent, linear phonon propagation rather than any thermal artifact.

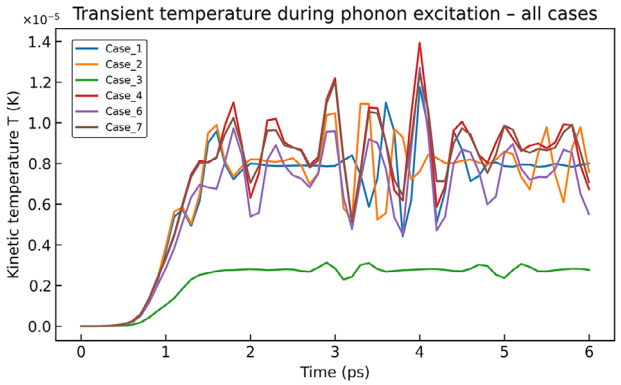

Figure 3. Transient kinetic temperature for cases 1–7. Each trace corresponds to the temp column extracted from LAMMPS logs. The envelope saturates below 2×10^{-5} K, indicating negligible heating.

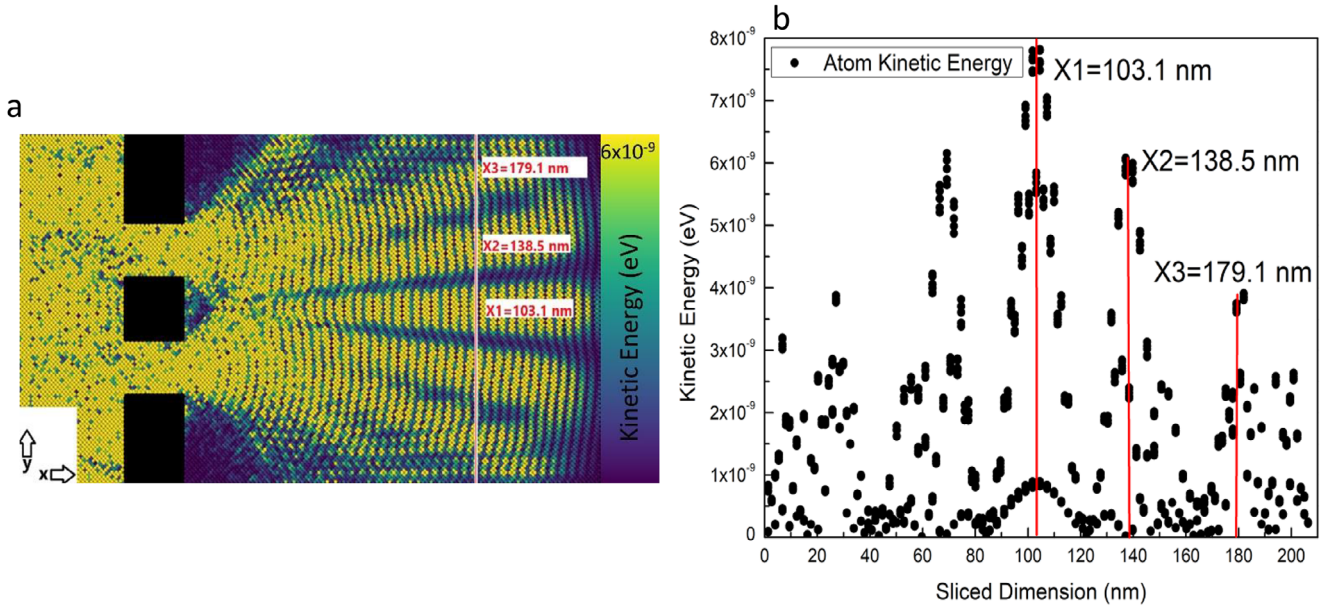

Figure 4. Time-averaged kinetic-energy map for Case 4 (slit spacing d = 4 nm, slit width c = 3 nm, slit length A = 4 nm). a) Colors indicate atomic kinetic energy on from $0 - 6 \times 10^{-9} eV$. The white vertical line marks the probe plane located $D = 20.27nm$ downstream of the slits. b) Scatter plot of atomic kinetic energy on that probe plane as a function of (y) position. Red guide lines highlight three constructive-interference peaks at $x1 = 103.1\ nm$, $x2 = 138.5\ nm$, and $x3 = 179.1\ nm$.

This allows to observe the interference and to study the effect of scattering only. With the frequency defined, the next step is adjusting the slit parameters and structural dimensions, aiming to investigate how the geometry can be manipulated to control and enhance the phononic wave behavior, potentially observing interference patterns akin to those in a double slit experiment. To provide context, it's important to note that the wavelength associated with longitudinal phonons in the (100) direction within crystalline silicon at a frequency of $6\ THz$ is $\approx 1.2\ nm$. This specific value has been derived from the dispersion relation of the potential used, employing the dynamical structure factor, as described in a prior research article.[40] Seven different geometric cases were studied (see Table 2) and for each there a continuous wave propagation happening. By systematically varying the slit length (A), the centre-to-centre slit distance (d), and the slit width (c), we correlate subtle geometric changes with their impact on phonon propagation and test whether a double-slit kind of interference emerges. The excitation is purely longitudinal, transverse modes did not produce a resolvable fringe pattern under identical conditions. Two of the three geometric parameters, (d) and (c), enter directly into the classical Young's fringe- spacing relation. Defining an effective slit distance (same as Young's case) as:

$$d' = d + c \tag{6}$$

the distance between adjacent "bright" fringes on a detection plane a distance D downstream is

$$e(D) = \frac{\Delta m \lambda D}{d'} \tag{7}$$

where λ is the phonon wavelength and as discussed previously its always $\lambda = 1.2\ nm$. Here $\Delta m = 1, 2, 3, 4$ but for this experiment is expected to reach up to 2 since further away fringes might not be measurable.

Direct comparison of the simulation data and the analytical solution of this formula solved for specific wavelength, slit distance and slit width, is the only possible way to compare the phenomenon with that of the equivalent case of light. For the frequency analysis wavelength was modified in each case ($1THz - 6THz$) and geometry was constant and for the geometric analysis wavelength was constant ($6THZ \approx 1.2\ nm$) and geometry varied slightly in each case (Table 1). Kinetic energy maps were extracted for the experimental process to be pre-evaluated, whether the interference phenomenon appears at all. From these 3D kinetic energy maps 2D slices of the material were generated as a scatter plot of kinetic energy versus the sliced dimension (y). The interference peaks expected are easily spotted on the scatter plot which was used to measure the distance between fringes. The sampling distances (12.27, 14.27, 16.27, 18.27, 20.27, 22.27, 24.27, 25.27 nm) were determined by the system geometry, with propagation distances spanning 37 nm to 50 nm with a step of 2 nm. For each sampling distance, the corresponding distance from the fixed slit position (24.73 nm) to the slab edge was calculated by converting the total slab dimensions and subtracting the slit position. This process was repeated for two distinct fringe orders (m values). Essentially the sampling distances correspond to 37.00, 39.00, 41.00, 43.00, 45.00, 47.00, 49.00, 50.00 nm at direction x (see **Figure 4**).

To assess the similarity between the phenomenon observed in silicon and the interference fringe distances in the double-slit photon experiment, they can be directly compared to theoretical predictions derived from Young's formula, focusing on the

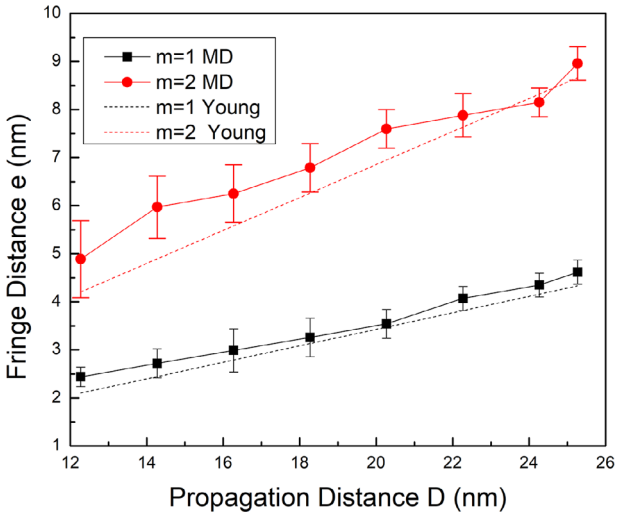

Figure 5. Direct comparison between the fringe spacing predicted by Young's double-slit formula (dotted lines) and that measured in the MD simulations of Case 4 ($d = 4$ *nm*, $c = 3$ *nm*). Black squares/red circles correspond to first-order ($m = 1$) and second-order ($m = 2$) fringes, respectively. The $m = 1$ data follow the linear Young's trend closely, whereas the $m = 2$ data deviate progressively with distance, reflecting the larger phase-noise sensitivity of higher-order fringes.

common variables d (center-to-center slit distance) and λ (wavelength). The evaluation draws on two complementary data sets (**Figure 5**). Simulation data consist of fringe spacings measured directly from the kinetic-energy maps produced by the MD runs (Figure 4a). Analytical data are the corresponding fringe spacings calculated from Young's relation (Equation (3), using the same detection-plane distance (D) and identical geometric parameters. Comparing these two sets quantifies how closely the simulated phonon patterns follow classical double-slit theory. The d' parameter which is effective slit distance from Young's formula include the other two investigated parameters d and c. In the optical analogue, slit length (A) is effectively not defined and thus absent from the classical analysis. Here we vary (A) just enough to check whether fringe formation is affected, rather than treating it as a primary comparative parameter.

Additionally, a direct comparison of the total kinetic energy transmitted through the system using configurations with identical aperture areas but different slit separations, specifically, Case 1 (d = 8.6 nm) and Case 4 (d = 4.0 nm) was conducted. The kinetic energy from MD trajectories at the previously mentioned distances (12.27–25.27 nm) were extracted and integrated the total vibrational energy across each slice. This comparison was conducted in an effort to confirm that coherent phonon interference modulates energy transport beyond geometry.

3. Results

Using the previously mentioned methodology, we visualize of the data (**Figure 6**) for first order fringes ($\Delta m = 1$) and second order fringes ($\Delta m = 2$). It can be observed that the molecular dynamics fringe distance is consistently increasing with the propagation of the wave. Because the Gaussian-ramped drive produces only 1.8×10^{-5} of strain, the lattice remains strictly harmonic. In parallel as mention in methodology the lattice remains effectively cryogenic, suppressing anharmonic phonon scattering and confirming that the observed interference patterns reflect purely coherent, linear dynamics.

From the solution of Equation (3) we already know the linearity between fringe distance and propagating distance with the gradient/slope being $\Delta m\lambda/d'$. For these measurements it appears that the second half of the plots are more uniform regarding the gradient of the phenomenon, on the other hand the closer the measurement is to the slits (smaller D) the more inconsistent change is observed to the fringe distance. This is predictable since the slits continue to leak energy through their walls into the system, thus creating more noise, preventing the measurement of the inter fringe distance. The geometric variables for each case were chosen in a way that always one of the three A, d, c variables are constant (Table 2) and for each case, there are a first (m = 1) and a second fringe (m = 2) distance.

In cases 1,2,3, d and c are kept constant with A taking the value 4 , 8 , 12 nm. In cases 4 and 5, A and c are constant and for cases 6 and 7, A and d, are constant. All the cases are displayed **Figure 7** as graphs of the distance the wave travelled axis) and the fringe distance (y axis). In Figure 7 are included both (MD) simulation data and analytical solution data of to identify similarities and patterns during the time progression of the phenomenon.

Increasing the slit width (c) from 1 to 5 nm decreases the distance of the fringes on every sampling step for first neighboring fringes ($\Delta m = 1$) and second neighboring fringes ($\Delta m = 2$). This is consistent with the analytical solution. The molecular dynamics results are getting more consistent with the theoretical for distance greater than 22.27 nm for $\Delta m = 1$ but for

$\Delta m = 2$ theory reports greater distances. Indeed, the analytical solution is given for an infinity small aperture. Increasing the slit distance (d) from 4 to 20 nm decreases the distance of the fringes on every sampling step for first neighboring fringes ($\Delta m = 1$) and second neighboring fringes ($\Delta m = 2$). Also, the same pattern is observed in the data extracted from the analytical solution. A slight offset between experimental and theoretical data exists for both the first and second neighboring fringes, that gets smaller as the wave propagates.

For first neighboring fringes ($\Delta m = 1$) at least based on these three cases with slit length (A) 4 , 8 , 12 nm respectfully, there is no observable concrete evidence of an underlying pattern (see **Figure 8**). For both small and large fringe distances, the fluctuation of the fringe distance seems to be small and can probably attributed to human measurement error. For second neighboring fringes ($\Delta m = 2$) close to the slits, it seems that the increase of the slit length A is decreasing fringe distance. As the wave gets further away from the slits the distance decrease gets smaller.

4. Conclusion

In this study, we successfully adapted the classic double-slit experiment, originally developed for light waves, to investigate the behavior of phonon waves in crystalline silicon. Through molecular dynamics (MD) simulations, we explored how phonons, can exhibit interference patterns when passing through two slits in a silicon block.

The results indicate that longitudinal acoustic waves behave similarly with photons, with distinct interference patterns emerg-

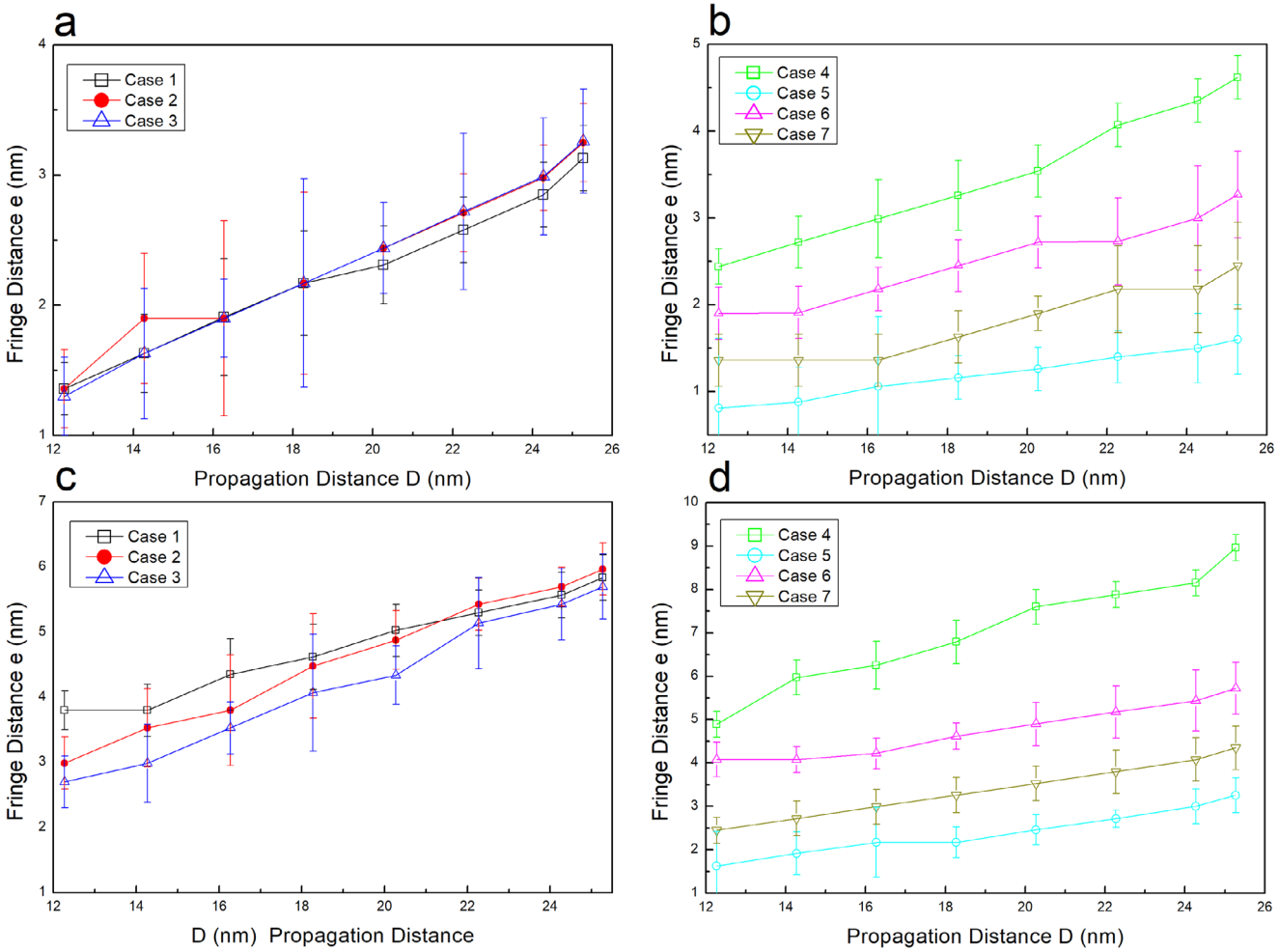

Figure 6. Fringe spacing extracted from the molecular-dynamics simulations for all seven geometries (error bars show ±1 SD over three independent slices at each detection plane). Panels a and b plot first-order fringes ($m = 1$), panels *c* and *d* plot second-order fringes ($m = 2$). Panels a and c share Cases 1–3, where slit spacing is fixed at $d = 8.6$ *nm* while slit length A is varied, panels b and d show Cases 4–7, where either slit distance d or slit width c is varied while $A = 4$ *nm*. In every case the fringe distance e increases approximately linearly with propagation distance D, consistent with Young's relation. Smaller effective slit separation (Cases 4–7) produces a steeper slope, and second-order fringes are systematically wider than first-order fringes.

ing from the simulations. The observed offset between the experimental and theoretical data diminishes as the wave propagates because the localized noise and distortions near the slits gradually dissipate, allowing the wavefront to stabilize and more closely resemble the idealized conditions assumed in the analytical model. Additionally, the decrease in fringe distance becomes smaller with increasing propagation distance due to the geometric spreading of the wavefront and the attenuation of energy density, which smooths out the interference pattern and reduces the influence of higher-order effects. These results underscore the dynamic interplay between real-world molecular dynamics simulations and theoretical predictions, highlighting how initial imperfections and finite aperture effects resolve over time to reveal patterns that increasingly align with the idealized framework of the Young's equation.

Together, these insights translate phononic interference into a concrete transport picture. By examining the kinetic-energy flux downstream of the slits, we observe pronounced instantaneous oscillations—alternating regions of high and low flux—that average out to a constant value under coherent drive. This demonstrates that interference does not remove energy but rather redistributes it spatially into narrow high-flux lobes and adjacent low-flux zones. Such controlled redistribution of vibrational energy highlights the potential to concentrate or divert heat at the nanoscale without net loss.

By carefully manipulating geometric parameters such as slit width, distance, and length, we were able to observe changes in fringe distances that align with theoretical predictions. The key findings include:

- Phonon Interference: We observed that phonons, much like light, create distinct interference patterns when propagating through nano-scale slits. These patterns can be manipulated by altering the geometric parameters of the system, such as slit width, distance, and length.

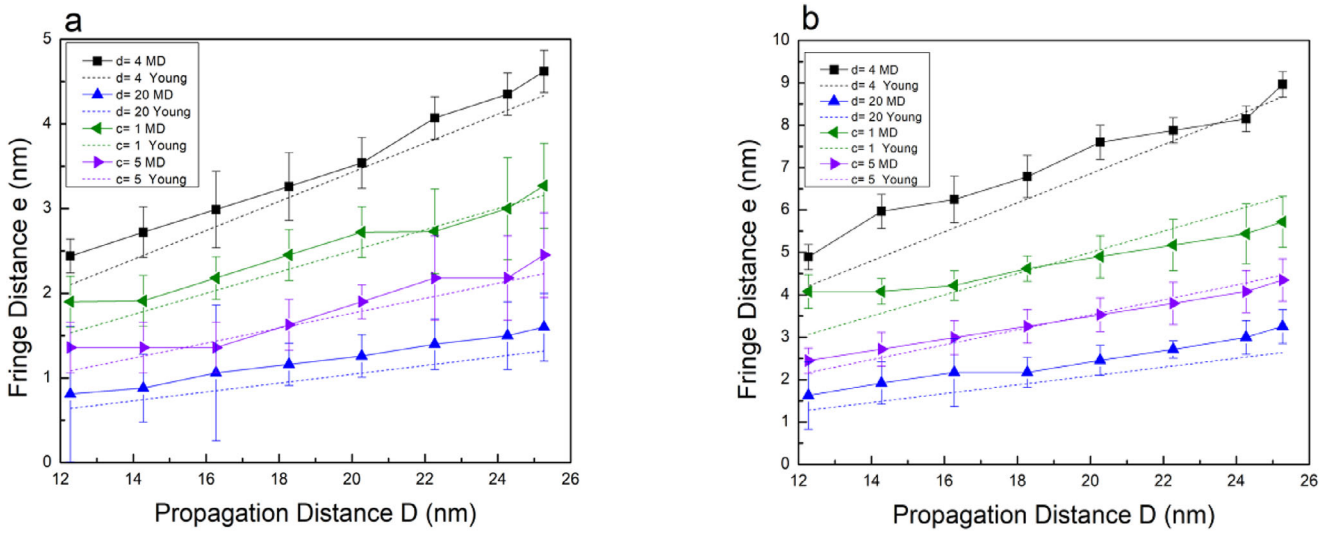

Figure 7. Multivariate comparison of simulated fringe distance with the Young-equation prediction for four representative geometries in which a single parameter is varied while the others are held fixed (A = 4 nm). Symbols with error bars are molecular-dynamics (MD) results and dotted lines are the corresponding Young's values. Black squares/blue triangles vary the slit spacing ($d = 4$ *nm* and $d = 20$ *nm*, respectively); green circles/magenta diamonds vary the slit width ($c = 1$ *nm* and $c = 5$ *nm*, respectively). a) First-order fringes ($m = 1$). b) Second-order fringes (m = 2). In every case the slope of $e(D)$ increases as the effective slit separation $d' = d + c$ decreases, and the MD data track the Young's prediction at each detection plane.

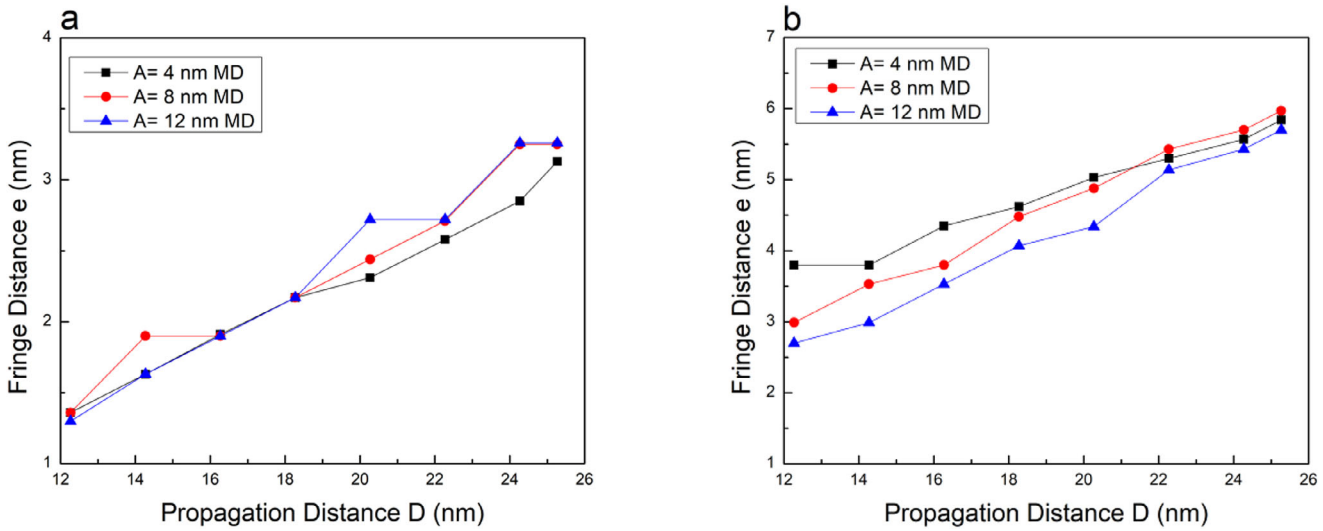

Figure 8. Influence of slit length A on phonon-interference fringe spacing. The slit spacing and width are fixed at $d = 8.6$ *nm* and $c = 3$ *nm*, while *A* is varied among 4, 8, and 12 *nm*. Symbols show molecular-dynamics values, lines are guides to the eye. a) First-order fringes ($m = 1$). b) Second-order fringes ($m = 2$). Fringe spacing $e(D)$ is essentially unchanged with *A*, indicating that interference is governed primarily by the transverse geometry (*d* and *c*), not by the slit length along the propagation direction.

- Geometric Influence: The distance between interference fringes is sensitive to changes in the geometric configuration of the slits. Specifically, increasing the slit width and distance led to measurable changes in the fringe patterns, confirming the theoretical predictions based on Young's formula.
- Frequency Selection: The simulations identified an optimal phonon propagation frequency (6 THz) at which the interference patterns were most clearly defined. This suggests that there is a specific phononic frequency range within silicon that maximizes wave coherence and interference.

Although the results generally align with theoretical expectations, noise in the MD simulations, particularly near the slits, caused deviations from the predicted fringe distances. In conclusion, our study demonstrates that phonon behaviour at the nanoscale can indeed mirror classical wave interference phenomena. From a practical standpoint, even single-frequency coherent interference offers a powerful tool to direct phonon energy distributions, on par with modulation achieved by alloying or interface roughness. In real devices with broadband phonon spectra, the aggregate effect will depend on coherence lengths and spec-

tral composition, but our idealized double-slit simulations establish a clear upper bound and quantitative benchmark. Extending these interference motifs into periodic or aperiodic multilayers would allow the redistribution effects to accumulate, providing a geometry-based complement to conventional scattering strategies in applications such as phononic lenses, thermal diodes, and guided-wave heat management.

Supporting Information

Supporting Information is available from the Wiley Online Library or from the author.

Acknowledgements

This work was supported by computational time granted from the Greek Research & Technology Network (GRNET) in the "ARIS" National HPC infrastructure under the project NOUS (pr017012).

Conflict of Interest

The authors declare no conflict of interest.

Author Contributions

E.N. led the project execution, adapted and expanded Dr. Desmarchelier's code for High-Performace Computing (HPC) systems, optimized LAMMPS scripts, designed geometries, conducted measurements, performed data analysis, error calculations, and created visual schematics and wrote this manuscript. P.D. Developed the foundational simulation code critical to the study, co-refined methodology, and contributed substantially to manuscript revisions. Y.N. provided essential theoretical frameworks through their pioneering prior research, which significantly influenced the foundational concepts and analytical approaches of this work. A.T. Contributed to the design of the project configurations, and with insightful discussions. K.T. originated the project vision, supervised all phases of research, and provided strategic guidance. J.K. Co-supervised the project, ensured resource allocation, provided continuous technical and organizational support throughout the study and contributed substantially to manuscript revisions.[41]

Data Availability Statement

The data that support the findings of this study are openly available in Zenodo at https://doi.org/10.5281/zenodo.15419412, reference number 15419412.

Keywords

atomistic simulations, molecular dynamics, phonon interference

Received: March 17, 2025
Revised: May 16, 2025
Published online: July 10, 2025

[1] J. Larmor, *Proc. Phys. Soc. Lond.* **1895**, *14*, 303.
[2] J. Bardeen, W. H. Brattain, *Phys. Rev.* **1948**, *74*, 230.
[3] M. Bass, P. A. Franken, J. F. Ward, G. Weinreich, *Phys. Rev. Lett.* **1962**, *9*, 446.
[4] L. A. Sterczewski, J. Mnich, J. Sotor, *Adv. Phys. Res.* **2025**, *4*, 2400105.
[5] M. Maldovan, *Nature* **2013**, *503*, 209.
[6] J. Zhang, H. Zhang, W. Li, G. Zhang, *Nanoscale Adv* **2023**, *5*, 5641.
[7] Y.-W. Seong, H. Kwon, C. Lee, H. Lim, K. Jeong, H. J. Shin, M.-H. Cho, *Adv. Funct. Mater.* **2025**, *35*, 2415462.
[8] D. Paparo, A. Martinez, A. Rubano, *J. Raman Spectrosc.* https://doi.org/10.1002/jrs.6787.
[9] G. Wehmeyer, T. Yabuki, C. Monachon, J. Wu, C. Dames, *Appl. Phys. Rev.* **2017**, *4*, 041304.
[10] S. Wang, A. L. Cottrill, Y. Kunai, A. R. Toland, P. Liu, W.-J. Wang, M. S. Strano, *Phys. Chem. Chem. Phys.* **2017**, *19*, 13172.
[11] L. Yadgarov, R. Tenne, *Small* 2400503.
[12] H. Song, S. Chen, X. Sun, Y. Cui, T. Yildirim, J. Kang, S. Yang, F. Yang, Y. Lu, L. Zhang, *Adv. Sci.* **2024**, *11*, 2403176.
[13] H. Liu, H. Wang, X. Zhang, *Appl. Sci.* **2019**, *9*, 344.
[14] H. Nakamura, N. Karasawa, *Nanoscale* **2025**, *17*, 7402.
[15] X. Huang, R. Anufriev, L. Jalabert, K. Watanabe, T. Taniguchi, Y. Guo, Y. Ni, S. Volz, M. Nomura, *Nature* **2024**, *634*, 1086.
[16] H. Kim, G. Park, S. Park, W. Kim, *ACS Nano* **2021**, *15*, 2182.
[17] Z. Xing, Y. Liu, N. Wu, S. Wang, X. Zhang, *Phys. Chem. Chem. Phys.* **2024**, *26*, 21727.
[18] D. J. Dieleman, A. F. Koenderink, A. F. M. Arts, H. W. de Wijn, *Phys. Rev. B.* **1999**, *60*, 14719.
[19] M. D. Losego, M. E. Grady, N. R. Sottos, D. G. Cahill, P. V. Braun, *Nat. Mater.* **2012**, *11*, 502.
[20] H. Wei, Y. Hu, H. Bao, *Commun. Mater.* **2023**, *4*, 3.
[21] L. M. Sandonas, R. Gutierrez, A. Dianat, G. Cuniberti, *RSC Adv.* **2015**, *5*, 54345.
[22] T. Çağın, J. B. Haskins, A. Kınacı, C. Sevik, in *Computational Materials, Chemistry, and Biochemistry: from Bold Initiatives to the Last Mile: In Honor of William A. Goddard's Contributions to Science and Engineering*, (Eds.: S. Shankar, R. Muller, T. Dunning, G. H. Chen), Springer International Publishing, Cham **2021**, pp. 451–479.
[23] M. N. Luckyanova, J. Garg, K. Esfarjani, A. Jandl, M. T. Bulsara, A. J. Schmidt, A. J. Minnich, S. Chen, M. S. Dresselhaus, Z. Ren, E. A. Fitzgerald, G. Chen, *Science* **2012**, *338*, 936.
[24] D. Chakraborty, H. Karamitaheri, L. de Sousa Oliveira, N. Neophytou, *Comput. Mater. Sci.* **2020**, *180*, 109712.
[25] G. Xie, D. Ding, G. Zhang, *Adv. Phys. X.* **2018**, *3*, 1480417.
[26] S. Li, X. Ding, J. Ren, X. Moya, J. Li, J. Sun, E. K. H. Salje, *Sci. Rep.* **2014**, *4*, 6375.
[27] M. Maldovan, *Nat. Mater.* **2015**, *14*, 667.
[28] A. Seif, W. DeGottardi, K. Esfarjani, M. Hafezi, *Nat. Commun.* **2018**, *9*, 1207.
[29] T. Young, *Philos. Trans. R. Soc. Lond.* **1804**, *94*, 1.
[30] P. Hariharan, *Rep. Prog. Phys.* **1991**, *54*, 339.
[31] J. Lee, In *1970 IEEE International Conference on Engineering in the Ocean Environment – Digest of Technical Papers*, IEEE, Piscataway, NJ **1970**, pp. 63–65.
[32] C. H. Anderson, E. S. Sabisky, *Phys. Rev. Lett.* **1970**, *24*, 1049.
[33] P. Desmarchelier, E. Nikidis, R. Anufriev, A. Tanguy, Y. Nakamura, J. Kioseoglou, K. Termentzidis, *J. Appl. Phys.* **2024**, *135*, 015103.
[34] Z. Zhang, Y. Guo, M. Bescond, J. Chen, M. Nomura, S. Volz, *Phys. Rev. Lett.* **2022**, *128*, 015901.
[35] P. Desmarchelier, E. Nikidis, J. Kioseoglou, Y. Nakamura, A. Tanguy, K. Termentzidis, In *2022 28th International Workshop on Thermal Investigations of ICs and Systems (THERMINIC)*, IEEE, Piscataway, NJ **2022**, pp. 1–4.
[36] P. Desmarchelier, A. Carré, K. Termentzidis, A. Tanguy, *Nanomaterials* **2021**, *11*, 1982.
[37] G. J. Martyna, D. J. Tobias, M. L. Klein, *J. Chem. Phys.* **1994**, *101*, 4177.

[38] R. L. C. Vink, G. T. Barkema, W. F. van der Weg, N. Mousseau, *J. Non-Cryst. Solids* **2001**, *282*, 248.
[39] G. P. Srivastava, *The Physics of Phonons*, Routledge, England, UK **2019**.
[40] P. Desmarchelier, A. Beardo, F. X. Alvarez, A. Tanguy, K. Termentzidis, *Int. J. Heat Mass Transf.* **2022**, *194*, 123003.
[41] E. Nikidis, P. Desmarchelier, Y. Nakamura, A. Tanguy, K. Termentzidis, J. Kioseoglou, Data: Exploring Phonon Interference: Insights from a Nano-Scale Silicon Double Slit Atomistic Simulation, Zenodo, **2025**. https://doi.org/10.5281/zenodo.15419412.